A&A 589, A21 (2016)
DOI: 10.1051/0004-6361/201628270

Astronomy & Astrophysics

K–H_2 line shapes for the spectra of cool brown dwarfs⋆

N. F. Allard[1,2], F. Spiegelman[3], and J. F. Kielkopf[4]

[1] GEPI, Observatoire de Paris, UMR 8111, CNRS, Université Paris VII, 61 avenue de l'Observatoire 75014 Paris, France
e-mail: nicole.allard@obspm.fr
[2] Institut d'Astrophysique de Paris, UMR 7095, CNRS, Université Paris VI, 75014 Paris, France
[3] Laboratoire de Chimie et Physique Quantique, UMR 5626, CNRS, Université Paul Sabatier, 118 route de Narbonne, 31400 Toulouse, France
[4] Department of Physics and Astronomy, University of Louisville, Louisville, Kentucky 40292, USA

Received 8 February 2016 / Accepted 24 February 2016

ABSTRACT

Observations of cooler and cooler brown dwarfs show that the contribution from broadening at many bars pressure is becoming important. The opacity in the red optical to near-IR region under these conditions is dominated by the extremely pressure-broadened wings of the alkali resonance lines, in particular, the K I resonance doublet at 0.77 μm. Collisions with H_2 are preponderant in brown dwarf atmospheres at an effective temperature of about 1000 K; the H_2 perturber densities reach several 10^{19} even in Jupiter-mass planets and exceed 10^{20} for super-Jupiters and older Y dwarfs. As a consequence, it appears that when the far wing absorption due to alkali atoms in a dense H_2 atmosphere is significant, accurate pressure broadened profiles that are valid at high densities of H_2 should be incorporated into spectral models.

Key words. line: profiles – brown dwarfs

1. Introduction

The cooling sequence of brown dwarfs has now been observationally characterized well beyond the transition from T to Y, or corresponding to effective temperatures down to 500 K or lower (Luhman 2014). Such objects are directly comparable to massive giant planets (super-Jupiters) around a Gyr in age or older and to the closest brown-dwarf analogs of Jupiter-mass planets at intermediate ages (Beichman et al. 2014). As a result of strong molecular and quasi-molecular absorption at longer wavelengths, among their spectral features best characterized from the ground are the near-infrared (NIR) flux peaks around 1 μm; these flux peaks are actually emerging from deep photospheric layers at temperatures around 1000 K and pressures of 10 to 100 bars.

Alkali–H_2 collisional profiles have been the subject of previous studies by Burrows & Volobuyev (2003) and Allard et al. (2003, 2007c,b). Absorption profiles of sodium and potassium perturbed by helium and molecular hydrogen were presented in Burrows & Volobuyev (2003) using multiconfiguration self-consistent field Hartree-Fock potentials in the Szudy theory (Szudy & Baylis 1975, 1996). Blue satellites on the line are predicted in the far wing of alkali-He/H_2 line profiles; such satellite bands of alkali metals perturbed by rare gas were extensively studied in the past (Allard & Kielkopf 1982 and references therein). A reliable determination of the line profiles that is applicable in all parts of the line at all densities is the Anderson semiclassical theory, which utilizes the Fourier transform of an autocorrelation function (Anderson 1952). In Allard et al. (2003, 2005), Allard & Spiegelman (2006), and Allard et al. (2007b), we used the molecular-structure calculations performed by Rossi & Pascale (1985; hereafter labeled RP85) for the molecular potentials of alkali–H_2 systems. This approach to calculating the spectral line profile requires the knowledge of molecular potentials with high accuracy because the shape and strength of the line profile are very sensitive to the details of the molecular potential curves describing the K–H_2 collisions. Ab initio calculations of the potentials of K–H_2 for different orientations of the molecule have been reported in Santra & Kirby (2005) and Allard et al. (2007c), neglecting the spin-orbit coupling (SO). In a previous paper (Allard et al. 1999), we derived a classical path expression for a pressure-broadened atomic spectral line shape that allows for an electric dipole moment that is dependent on the position of perturbers, which is not included in the more usual approximation of Anderson & Talman (1956) and Baranger (1958a,b). This treatment has improved the comparison of synthetic spectra of brown dwarfs with observations (Allard et al. 2003, 2007a).

In Sect. 2 we describe new calculations of the K–H_2 potential energy surfaces in which the two electrons of H_2 and the valence electron of potassium are explicit. The improvement over our previous work (Allard et al. 2007b) consists in a better determination of the intermediate and long range part of the K–H_2 potential and inclusion of spin-orbit coupling, which enables a new determination of the line widths of the two components of the doublet (Sect. 3).

In this continuation of previous work (Allard et al. 2003, 2007c), we illustrate the evolution of the absorption spectra of K–H_2 collisional profiles for the densities and temperatures

⋆ The opacity tables are only available at the CDS via anonymous ftp to cdsarc.u-strasbg.fr (130.79.128.5) or via http://cdsarc.u-strasbg.fr/viz-bin/qcat?J/A+A/589/A21

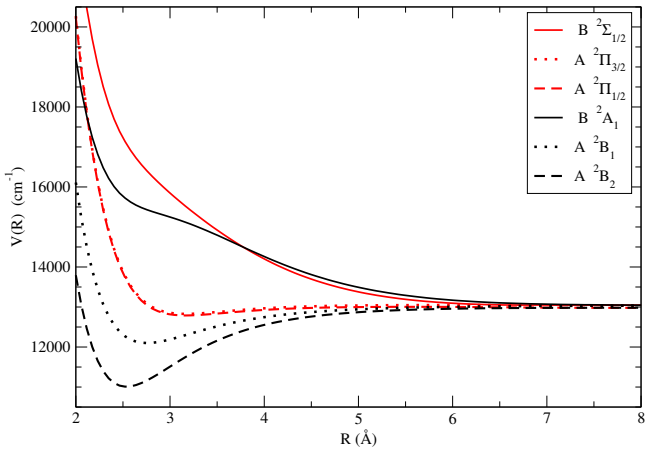

Fig. 1. Potential curves for the A and B states of the K–H_2 molecule for the $C_{\infty v}$ (red curves) and C_{2v} symmetries (black curves).

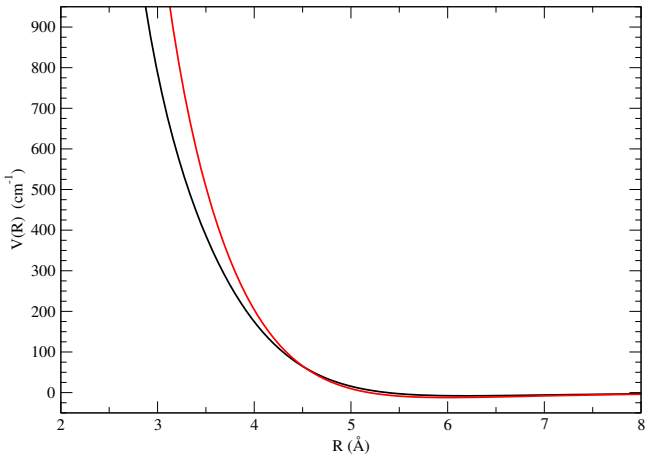

Fig. 2. Potential curves for the X state of the K-H_2 molecule for the $C_{\infty v}$ (red curves) and C_{2v} symmetries (black curves).

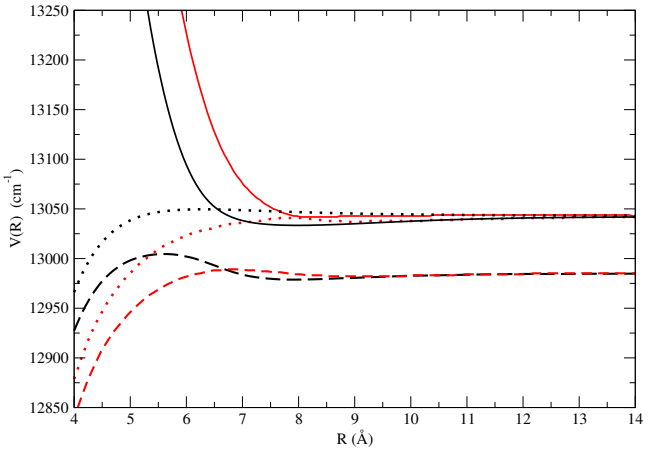

Fig. 3. Ab initio potentials (black curves) for the $C_{\infty v}$ symmetry compared at intermediate and long range internuclear distance with the pseudo-potential results of Rossi & Pascale (1985; red curves); B (full line), A $P_{3/2}$ (dotted line), and A $P_{1/2}$ (dashed line).

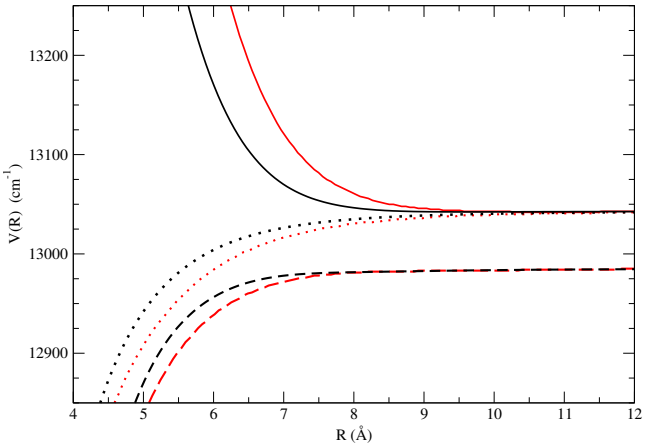

Fig. 4. Ab initio potentials (black curves) for the C_{2v} symmetry compared with the pseudo-potential results of Rossi & Pascale (1985; red curves); B $^2A_1$ (full line), A $^2B_1$ (dotted line), and A $^2B_2$ (dashed line).

prevailing in atmosphere of cool brown dwarf stars (Sect. 4). Laboratory measurements are used to validate the new ab initio molecular potentials presented here, and to confirm their implementation in the spectral line profile theory (Sect. 5).

2. K–H_2 diatomic potentials including spin-orbit coupling

We carried out the ab initio calculations of the potentials (hereafter labeled S15) for the C_{2v} (T-shape) symmetry group and the $C_{\infty v}$ (linear) symmetry group in a wide range of distances R between the K atom and the center of mass of the molecule H_2 (Figs. 1–4).

In the calculation of the complex, we kept the bond length of H_2 fixed at the equilibrium value r_e = 1.401 a.u. and the approach is along the z coordinate axis. We followed the same electronic structure calculation schemes as in our previous work (Allard et al. 2007c) on KH_2, namely a pseudo-potential description of the potassium atom core complemented by a core polarization operator to include the core response. The pseudo-potential expressions and Gaussian type basis sets (GTOs) were already published (Allard et al. 2007c). In the former work (Allard et al. 2007c), we had considered configuration interaction (CI) in determinantal spaces generated from a multireference MRPT2 perturbative scheme (Huron et al. 1973), retaining in a final variational CI all determinants with a contribution in the first-order wavefunction larger than 10^{-5} (the reference space itself included all single excitations with respect to the ground state configuration). This provided a result that could be considered a quasi-full CI for the three electrons with a residual perturbation less than 10 cm^{-1}. However, we noticed some noise in the potential energy definition along the K–H_2 separation distance grid, which was due to the fact that despite the use of a unique threshold, the selection process was achieved at each distance separately; this did not ensure the continuity of CI spaces from one distance to the next and, thus, generated noise. This was not too serious far from the line center, but could be problematic in the vicinity of the atomic line, namely at intermediate and long distances where the hydrogen influence is small and constant accuracy is required. In order to solve this problem, we thus (i) still reduced the selection threshold, setting it to 0.5×10^{-5}; and (ii) merged the CI determinantal selections at all distances, performing the final CI with the final overall selection.

The spin-orbit coupling energy splitting $^2P_{\frac{3}{2}} - ^2P_{\frac{1}{2}}$ in the 4p level of potassium is 57.72 cm^{-1} (Moore 1971). Since we

want to address spectral regions close to the line center, we also incorporated SO coupling within a variant of the atom-in-molecule-like scheme introduced by Cohen & Schneider (1974). This scheme relies on a monoelectronic formulation of the spin-orbit coupling operator

$$H_{\rm SO} = \sum_i h_{\rm SO}(i) = \sum_i \zeta_i \hat{l}_i.\hat{s}_i. \quad (1)$$

The total Hamiltonian $H_{\rm el} + H_{\rm SO}$ is expressed in the basis set of the eigenstates (here with $M_{\rm s} = \pm\frac{1}{2}$) of the purely electrostatic Hamiltonian $H_{\rm el}$. The spin-orbit coupling between the molecular many-electron doublet states $\Phi_{k\sigma}$, approximated at this step as single determinants with the same closed shell $\sigma_{\rm g}^2$ H_2 subpart, is isomorphic to that between the singly occupied molecular spin-orbitals $\phi_{k\sigma}$, correlated with the six p spin-orbitals of the alkali atom (k labels the space part and $\sigma = \alpha, \beta$ labels the spin projection). The Cohen and Schneider approximation consists in assigning these matrix elements to their asymptotic (atomic) values

$$\langle \Phi_{k\sigma}|H_{\rm SO}|\Phi_{l\tau}\rangle = \langle \phi_{k\sigma}(\infty)|h_{\rm SO}|\phi_{l\tau}(\infty)\rangle. \quad (2)$$

The scheme makes no a priori assumption about the magnitude of spin-orbit coupling versus pure electrostatic interactions and enables general intermediate coupling. The effective spin-orbit integral of the $4p$ shell of potassium is taken empirically as 2/3 times the spin-orbit splitting, namely $\zeta_{4p} = 38.48$ cm^{-1}.

The main question for the applicability of this scheme in a basis of adiabatic states is the transferability of the atomic SO integrals to the molecular case. The situation can be problematic in the case where the molecular orbitals and/or the CI states undergo significant change and, thus, loose their asymptotic character. In order to improve the transferability of the Cohen-Schneider scheme, we thus implemented it within a diabatic representation scheme. Namely, we achieved a diabatization of the CI adiabatic states (Cimiraglia et al. 1985), obtaining quasi-diabatic states from a unitary transformation of the adiabatic states. The quasi-diabatic states $\tilde{\Phi}_k$ (omitting spin mention for convenience at this stage) at a given distance R are obtained by maximizing their overlaps with the asymptotic references, which are defined as the adiabatic states at infinite separation (here $R = 50\ a_0$), i.e., the quasi-diabatic states $\tilde{\Phi}_k$ are defined such that

$$\sum_k \langle \tilde{\Phi}_k(R)|\Phi_k(\infty)\rangle \quad (3)$$

is maximum at each distance R. This criterion ensures that, within a truncated manifold of states, the quasi-diabatic states resemble their asymptotic counterparts as much as possible. This process is achieved here including all molecular states correlated with 4s, 4p, and 5s asymptotes, which means that for the symmetries under consideration here, the transformation only affects the three states correlated with the 4s, 4pz, and 5s orbitals, namely $^2\Sigma^+$ states in symmetry $C_{\infty v}$ and $^2A_1$ states in symmetry C_{2v}. Within the unitary-transformed basis, the electronic Hamiltonian is thus no longer diagonal, but its diagonalization yields the same adiabatic energies as initially obtained in the CI process and from which it is unitary transformed. We hereafter designate $E_{\rm 4s}$, $E_{\rm 4px}$, $E_{\rm 4py}$, $E_{\rm 4pz}$, and $E_{\rm 5s}$ the diabatic energies of the states (diagonal elements). In the present case, states with orbitals perpendicular to the approach axis have identical adiabatic and diabatic energies (these states are single in their respective symmetries). Hereafter, $V_{\rm 4s4p}$, $V_{\rm 4s5s}$ and $V_{\rm 4p5s}$ label the off-diagonal elements of the electronic Hamiltonian obtained from diabatization of the $^2\Sigma^+$ or $^2A_1$ manifolds.

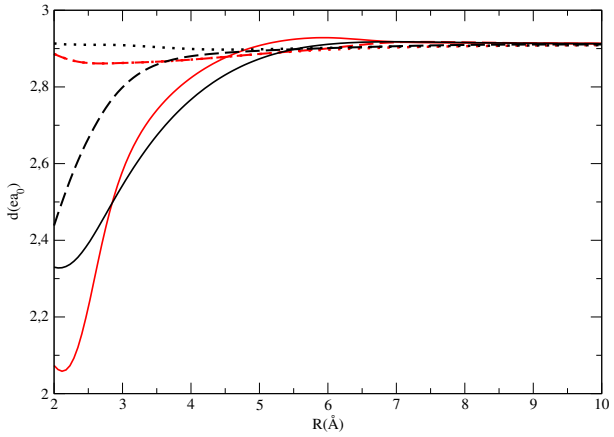

Fig. 5. Transition dipole moment for the B–X (full line), A $^2P_{3/2}$–X (dotted line), and A $^2P_{1/2}$–X (dashed line) transitions of the K–H_2 molecule for the $C_{\infty v}$ (red curves) and C_{2v}symmetries (black curves); B–X (full line), A $^2P_{3/2}$–X (dotted line), and A $^2P_{1/2}$–X (dashed line).

The total Hamiltonian matrix $H = H_{\rm el} + H_{\rm SO}$ is a 10×10 complex matrix written in the basis of the diabatic states components $\tilde{\Phi}_{k\sigma}$

$$\begin{pmatrix}
E_{\rm 4s} & 0 & 0 & 0 & 0 & 0 & V_{\rm 4s4p} & 0 & V_{\rm 4s5s} & 0 \\
0 & E_{\rm 4s} & 0 & 0 & 0 & 0 & 0 & V_{\rm 4s4p} & 0 & V_{\rm 4s5s} \\
0 & 0 & E_{\rm 4px} & 0 & -i\frac{\zeta}{2} & 0 & 0 & \frac{\zeta}{2} & 0 & 0 \\
0 & 0 & 0 & E_{\rm 4px} & 0 & i\frac{\zeta}{2} & \frac{\zeta}{2} & 0 & 0 & 0 \\
0 & 0 & i\frac{\zeta}{2} & 0 & E_{\rm 4py} & 0 & 0 & -i\frac{\zeta}{2} & 0 & 0 \\
0 & 0 & 0 & -i\frac{\zeta}{2} & 0 & E_{\rm 4py} & -i\frac{\zeta}{2} & 0 & 0 & 0 \\
V_{\rm 4s4p} & 0 & 0 & \frac{\zeta}{2} & 0 & i\frac{\zeta}{2} & E_{\rm 4pz} & 0 & V_{\rm 4p5s} & 0 \\
0 & V_{\rm 4s4p} & \frac{\zeta}{2} & 0 & i\frac{\zeta}{2} & 0 & 0 & E_{\rm 4pz} & 0 & V_{\rm 4p5s} \\
V_{\rm 4s5s} & 0 & 0 & 0 & 0 & 0 & V_{\rm 4p5s} & 0 & E_{\rm 5s} & 0 \\
0 & V_{\rm 4s5s} & 0 & 0 & 0 & 0 & 0 & V_{\rm 4p5s} & 0 & E_{\rm 5s}
\end{pmatrix}$$

The diagonalization of the above matrix at each internuclear distance provides the spin-orbit eigenstates Ψ_m^{SO} (spanned by coefficients $c_{k\sigma}^m$ on the diabatic states) and energies. Figures 1–4 present the potential energy surfaces $V_{\rm e}[R(t)] = E_{\rm e}[R(t)] - E_{\rm e}^{\infty}$ in the $C_{\infty v}$ and C_{2v} symmetries.

The transition dipole moments (Fig. 5) between the spin-orbit states Ψ_m^{SO} can be easily determined from those computed between the diabatic CI wavefunctions

$$\mathbf{D}_{mn}^{\rm SO} = \langle \Psi_m^{\rm SO}|\mathbf{D}|\Psi_n^{SO}\rangle = \sum_{k\sigma,l\tau} c_{k\sigma}^m c_{l\tau}^n \langle \tilde{\Phi}_{k\sigma}|\mathbf{D}|\tilde{\Phi}_{l\tau}\rangle \delta_{\sigma\tau}. \quad (4)$$

3. Spectral line parameters

The T-type brown dwarf optical spectra are totally controlled by the wings of the most abundant Na I D and K I resonance doublet perturbed by H_2, the most abundant form of hydrogen in these deepest, hottest photospheric layers. The cores, on the other hand, are formed in the uppermost, lowest density atmospheric layers dominated by H_2 collisions. Since in a model atmosphere calculation, the resulting line profile is the integration of the flux in all layers from the deepest to the uppermost, it is important that the centers be adequately represented; i.e., they can be non-Lorentzian at the high densities of the innermost layers, while Lorentzian in the upper atmosphere but with different widths than predicted by the hydrogenic van der Waals approximation usually used for the cores (Schweitzer et al. 1996).

In Allard et al. (2007b), spectral line widths of the light alkalies perturbed by He and H_2 were presented for conditions prevailing in brown dwarf atmospheres. We used the

molecular-structure calculations performed by Pascale (1983) for the adiabatic potentials of alkali-metal–He systems, and by Rossi & Pascale (1985) for the molecular potentials of alkali-H_2 systems. For that purpose, the fine structure was included in these potentials within the atom-in-molecule-like scheme introduced by Cohen & Schneider (1974) (see Sect. 2). In Fig. 6, we plotted the results obtained in the semiclassical unified theory using the potentials presented in Figs. 1–4. It shows the sensitivity of the half-width to the potentials.

The line widths w (HWHM) are linearly dependent on H_2 density and a power law in temperature given for the $^2P_{1/2}$ transition by

$$w = 0.1678 \times 10^{-20} n T^{0.3466} \quad (5)$$

and for the $^2P_{3/2}$ transition by

$$w = 0.2319 \times 10^{-20} n T^{0.3426}. \quad (6)$$

The nonlinear dependence on temperature is illustrated in Fig. 6. These expressions may be used to compute the widths for temperatures of stellar or planetary atmospheres from 400 to at least 4000 K.

H_2 collisions are preponderant in brown dwarf atmospheres and the broadening due to H_2 is larger than that due to He. We are not aware of other calculations of half-widths due to K–H_2 collisions. We could only compare the accurate theory with the broadening that is obtained from a van der Waals potential (vdW) in Fig. 6.

When it is assumed that the main interaction between two atoms is the long range van der Waals interaction of two dipoles, the Lindholm-Foley theory gives the usual formulae for the width and shift. The van der Waals damping constant is calculated according to the impact theory of the collision broadening.

A few laboratory experiments have measured the width, shift, and asymmetry of the light alkalis broadened by He at low density. For the most part, the alkali resonance lines are so narrow under laboratory conditions that a measurement of their widths requires extremely high spectral resolution and careful allowance for instrumental effects. Furthermore, because the shifts are also small, extremely good stability is required to make an accurate measurement of the dependence of shift on broadening, a process that requires measuring the wavelength of the line over a range of gas densities. Recently published experimental measurements for broadening by H_2 concerns neutral Na perturbed by H_2 (Allard et al. 2012b).

4. Spectral line absorption

The theory of spectral line shapes, especially the unified approach we developed, makes possible accurate models of stellar spectra that account both for the centers of spectral lines and their extreme wings in one consistent treatment. Complete details and the derivation of the theory are provided by Allard et al. (1999).

The blue satellites in the far wing of alkali–He/H_2 line profiles are correlated with the maxima in the difference potentials ΔV for the B–X transition (Allard et al. 2003, 2005, 2007c; Allard & Spiegelman 2006; Zhu et al. 2005, 2006). Details on the properties of the K–H_2 quasi-molecular line satellite have been reported in Allard et al. (2003, 2007c). The main difference between our previous work reported in Allard et al. (2003) was to predict a K–H_2 quasi-molecular line satellite closely matching the position and shape of an observed feature in the spectrum of the T1 dwarf ε Indi Ba. Ab initio calculations of the potentials of

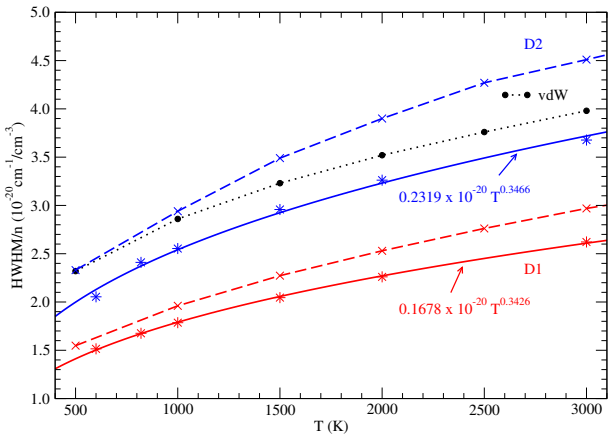

Fig. 6. Variation with temperature of the half-width of the D2 (blue curves) and D1 (red curves) lines of K I perturbed by H_2 collisions. New ab initio potentials (full line) and pseudo-potentials of Rossi & Pascale (1985; dashed lines), van der Waals potential (black dotted lines).

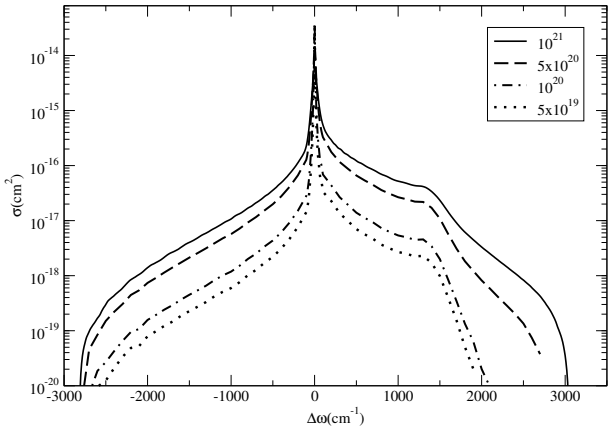

Fig. 7. Variation with the density of H_2 of the $D2$ component. The temperature is 1000 K.

K–H_2 (Allard et al. 2007c) enabled a better agreement with the observations (Allard et al. 2007a).

The density effect on the shape of the blue wing is very significant when the H_2 density becomes larger than 10^{20} cm^{-3}. Because of multiple perturber effects, we can notice in Fig. 7 a first line satellite at 1300 cm^{-1} and a second line satellite due to K–$(H_2)_2$ that appears as a shoulder about 2700 cm^{-1}. The density dependence of the far blue wing is no longer linear. Opacity tables of K–H_2, which can be incorporated into atmosphere calculations, are valid for perturber densities lower than 10^{20} cm^{-3}. Our line profiles that are valid at higher density need to be used to construct new tables.

Figures 8–9 present the variation with temperature of line profiles calculated for a fixed molecular hydrogen density $n_{H_2} = 10^{21}$.

5. Unified profiles compared to laboratory spectra

We measured the absorption spectrum of K with H_2 at pressures under 1 bar under controlled conditions in the laboratory to compare with the unified theory calculations and validation of the new potentials. In previous experimental and theoretical work on Na perturbed by H_2, we also reported the Na-line wings measured similarly (Allard et al. 2012a,b). We also reported the experimental methods for measurement of the line wings. As in

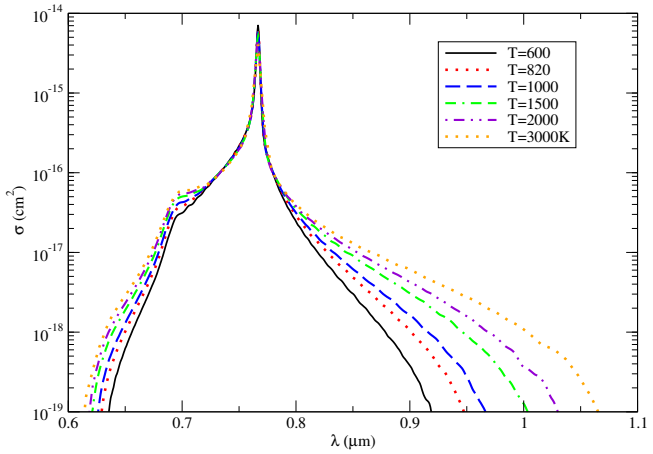

Fig. 8. Variation with temperature of the D2 component of the K I resonance doublet perturbed by H_2. The density of perturbers is $n_{H_2} = 10^{21}$ cm^{-3}.

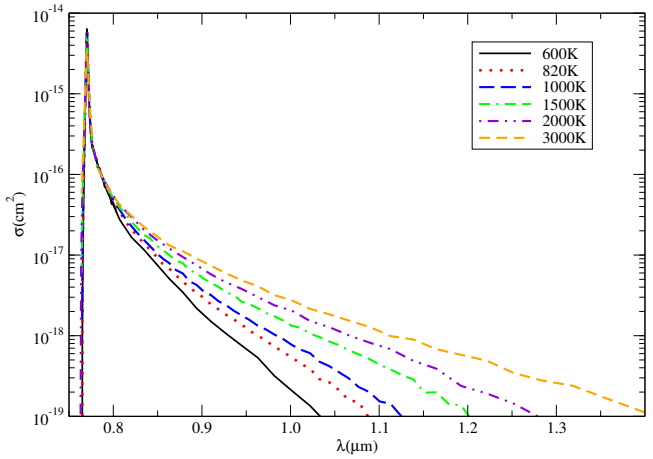

Fig. 9. Variation with temperature of the D1 component of the K I resonance doublet perturbed by H_2. The density of perturbers is $n_{H_2} = 10^{21}$ cm^{-3}.

that work, the data we report on here are from a series of spectra taken of a K absorption cell with a 30 cm long by 2.2 cm diameter uniformly heated central section.

The room temperature cell was flushed with He, loaded with 99.95% pure K metal, evacuated to 10^{-3} Torr with a mechanical pump, and also flushed with H_2 and heated to remove adsorbed water and volatile impurities. H_2 was introduced to the evacuated clean cell at 320 K, which was then sealed at an initial pressure on the order of 500 Torr. The cell temperature was monitored with thermocouples to an accuracy of 1 K, and the gas pressure was measured with a capacitive manometer accurate to ±1 Torr as indicators of a stable environment and to insure there was no significant additional outgassing or leaks while spectral data were collected. The absorption coefficient measurements reported here are in a regime of linear dependence on H_2 and K density.

A stable tungsten filament light source illuminated the entrance window of the cell through the output of a quasi-collimated fiber optical bundle, and transmitted light from the exit window of the cell was collected and sent through an optical fiber to a Czerny-Turner spectrometer, thus providing a first order dispersion of 4.3 Å per pixel on a Peltier-cooled Kodak (now On Semiconductor) KAF-0402E CCD sensor. This low resolution is ideal for a comprehensive survey measurement of the extended K-line wing. We have not measured the Lorentzian core in this work, and focus our attention on the line wing where critical information about the potentials is clearly distinguished. Once raw images were acquired, they were processed by subtracting dark frames and the spectra were extracted from selected regions summed over pixels at the same wavelength. Wavelength calibration against a Hg standard was applied and the 2-pixel resolution of the resulting spectra was approximately 8.6 Å or 15 cm^{-1} over the region of interest in the K-line wing.

The measured absorption signal was given by

$$I(\overline{\nu}) = I_0(\overline{\nu}) f(\overline{\nu}) \exp(-k(N_{H_2}, N_K, \overline{\nu})), \quad (7)$$

where I_0 is the background and f is the instrument response including spectrograph transmission and CCD efficiency. We made measurements at an elevated temperature where the density of K vapor was sufficient to produce absorption, and at room temperature where there was no absorption, that is where $k = 0$. The ratio of the two measurements eliminated the unknown background and sensitivity factors, effectively flat-fielding the spectra and yielding the absorption coefficient k at temperature T from Eq. (7). We cannot directly measure the absolute absorption cross section because the K number density is not independently known in this method. Furthermore, it was evident from the spectra that there was significant absorption from the K_2 molecule that is experimentally unavoidable at temperatures of interest. We also took data with Kr buffer gas, which will be reported elsewhere Kielkopf & Allard (in prep.), to remove this molecular background and reveal only the atomic K–H_2 spectrum. Kr, and all rare gases other than He, have classically inaccessible line wing contributions to the spectral region where the singular K–H_2 feature occurs, and therefore provide an absorption coefficient only due to K_2. It is straightforward then to remove this component by subtraction and leave only the coefficient of absorption due to K–H_2 in the reduced experimental data.

The result is shown in Fig. 10 for an H_2 density of 10^{19} cm^{-3} at 820 K. The experimental absorption spectrum is linearly scaled to match the theoretical total absorption. A point to note is that the wavelength of the maximum "satellite" feature is the same in both experiment and line shape theory. Although the satellite is broad, the nonclassical region (below 0.69 μm) decreases in strength exponentially and makes a sharply defined shoulder. The experimental data and theoretical profile follow this decrease exactly, within an uncertainty on the order of the spectral bandwidth of ±15 cm^{-1}. The nonclassical region beyond the satellite (toward the blue) follows the theory exactly into the noise floor of the measurement. The wavelength of the satellite is largely dependent on the accuracy of the potential difference of the two contributing states to the transition, while the strength of the absorption as a function of wavelength is dependent on the radial scaling of the potential, the radiative dipole moment shown in Fig. 5, and the accuracy of the spectral line shape theory. The region is clearly far different from a Lorenztian, and the shape of the satellite is not the same as given by simplified theories that do not treat core and wing in a unified way. While the effects seem small since they are a fraction of the total line strength far from the unperturbed line center, for light passing through H_2 with a long path length of K, the exponential absorption saturates the line center and the spectrum of the escaping radiation is defined by these otherwise subtle effects.

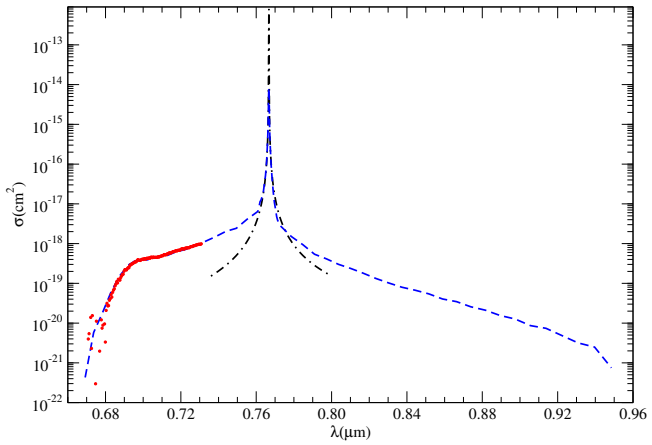

Fig. 10. Comparison of the theoretical profile (dashed blue line) of the D2 component with experimental absorption profile (dotted red line). The corresponding Lorentzian profile is overplotted (dash-dotted black line). The density of perturbers is $n_{H_2} = 10^{19}$ cm^{-3}, $T = 820$ K.

6. Conclusion

Ultracool stellar atmospheres show absorption by alkali resonance lines significantly broadened by collisions with neutral perturbers. In the coolest and densest atmospheres, such as those of T dwarfs, Na I and K I broadened by H_2 and by He can come to dominate the entire optical spectrum (Burrows et al. 2000). We have performed a theoretical determination of the K I–H_2 line profiles using a semiclassical collision approach and high quality ab initio potentials. The new models were confirmed by a laboratory measurement in a critical sensitive region on the short wavelength side of the resonance doublet where there is some emission in a typical brown dwarf atmosphere.

Opacity tables were constructed; the complete tables are available on request and at the CDS.

References

Allard, N. F., & Kielkopf, J. F. 1982, Rev. Mod. Phys., 54, 1103
Allard, N. F., & Spiegelman, F. 2006, A&A, 452, 351
Allard, N. F., Royer, A., Kielkopf, J. F., & Feautrier, N. 1999, Phys. Rev. A, 60, 1021
Allard, N. F., Allard, F., Hauschildt, P. H., Kielkopf, J. F., & Machin, L. 2003, A&A, 411, 473
Allard, N. F., Allard, F., & Kielkopf, J. F. 2005, A&A, 440, 1195
Allard, F., Allard, N. F., Homeier, D., et al. 2007a, A&A, 474, L21
Allard, N. F., Kielkopf, J. F., & Allard, F. 2007b, Eur. Phys. J. D, 44, 507
Allard, N. F., Spiegelman, F., & Kielkopf, J. F. 2007c, A&A, 465, 1085
Allard, N. F., Kielkopf, J. F., Spiegelman, F., Tinetti, G., & Beaulieu, J. P. 2012a, in EAS Pub. Ser., 58, 239
Allard, N. F., Spiegelman, F., Kielkopf, J. F., Tinetti, G., & Beaulieu, J. P. 2012b, A&A, 543, A159
Anderson, P. W. 1952, Phys. Rev., 86, 809
Anderson, P. W., & Talman, J. D. 1956, Bell System Tech. Rep., 3117 (Murray Hill, NJ)
Baranger, M. 1958a, Phys. Rev., 111, 481
Baranger, M. 1958b, Phys. Rev., 111, 494
Beichman, C., Gelino, C. R., Kirkpatrick, J. D., et al. 2014, ApJ, 783, 68
Burrows, A., & Volobuyev, M. 2003, ApJ, 583, 985
Burrows, A., M. S. Marley, M. S., & Sharp, C. M. 2000, ApJ, 531, 438
Cimiraglia, R., Malrieu, J.-P., Persico, M., & Spiegelmann, F. 1985, J. Phys. B, 18, 3073
Cohen, J. S., & Schneider, B. 1974, J. Chem. Phys., 61, 3230
Huron, B., Malrieu, J. P., & Rancurel, P. 1973, J. Chem. Phys., 58, 5745
Luhman, K. L. 2014, ApJ, 786, L18
Moore, C. E. 1971, National Standard Reference Data Series, NSRDS 35 Vol. I Atomic Energy Levels as Derived from the Analyses of Optical Spectra, Vol. I. 1H to 23V, NSRDS-NBS 35, 358, NSRDS 35 Vol. II Atomic Energy Levels as Derived from the Analyses of Optical Spectra, Vol. II. 24Cr to 41Nb, NSRDS-NBS 35, 263, NSRDS 35 Vol. III Atomic Energy Levels as Derived from the Analysis of Optical Spectra. Volume III. 42 Mo to 57La, 72Hf to 89Ac, NSRDS-NBS 35, 289
Pascale, J. 1983, Phys. Rev. A, 28, 632
Rossi, F., & Pascale, J. 1985, Phys. Rev. A, 32, 2657
Santra, R., & Kirby, K. 2005, J. Chem. Phys., 123, 214309
Schweitzer, A., Hauschildt, P. H., Allard, F., & Basri, G. 1996, MNRAS, 283, 821
Szudy, J., & Baylis, W. 1975, J. Quant. Spectrosc. Rad. Transfer, 15, 641
Szudy, J., & Baylis, W. 1996, Phys. Rep., 266, 127
Zhu, C., Babb, J. F., & Dalgarno, A. 2005, Phys. Rev. A, 71, 052710
Zhu, C., Babb, J. F., & Dalgarno, A. 2006, Phys. Rev. A, 73, 012506